LPS-stimulated liver section (Fig. 5C: middle). On the other hand, the destruction of hepatic central vein induced by LPS-stimulation was significantly suppressed by ICAM-1 siRNA delivery using Man-PEG_{2000} BLs and US exposure (Fig. 5C: right); suggesting that the liver injury induced by LPS-stimulation is suppressed by this siRNA delivery. Similar effects by this ICAM-1 siRNA delivery were also observed for CCl_4- and DMN-induced inflammatory mouse models (Supplementary Figs. 6C, 6D, 7C, and 7D).

Anti-inflammatory effects against IR-liver injury. The effects of ICAM-1 suppression by delivery of siRNA was evaluated for IR-liver injury (Fig. 6A). As shown in Figs. 6B and 6C, ICAM-1 expression induced by IR-stimulation was suppressed by siRNA delivery using Man-PEG_{2000} BLs and US exposure. Moreover, IL-8/MCP-1 expression and pro-inflammatory cytokine production were also suppressed (Figs. 7B and 7C). Following the examination of liver toxicity, ALT/AST activities in the serum and hepatic apoptosis were significantly suppressed (Figs. 8A and 8B). Moreover, following H&E-staining of liver sections, the circular and tube formations of hepatic central vein in normal liver (Fig. 8C: left) section is destructed by IR-stimulation (Fig. 8C: middle), on the other hand, IR-derived destruction of hepatic central vein was suppressed by this ICAM-1 siRNA delivery (Fig. 5C: right).

Discussion

In the sonoporation method, transient pores are created on the cell membrane followed by the destruction of microbubbles, and a large amount of nucleic acids can be directly transferred into the cytoplasm [21,26,27]. Since siRNA is functionalized in the cytoplasm, gene transfer using Man-PEG_{2000} BLs and US exposure [23-26] would be also suitable for

siRNA delivery. In the present study, we applied this gene transfer method for the selective and efficient delivery of siRNA to HECs *in vivo,* and investigated the anti-inflammatory effects in various types of inflammatory responses.

The innate inflammatory responses based on the interaction with siRNA and Toll-like receptors (TLRs)-3, -7, -8 should be excluded for evaluating the gene suppression effects of siRNA, but should be considered for clinical applications of siRNA [28,29]. The pro-inflammatory cytokines, such as TNF-α, IFN-γ, and IL-6, can be induced by siRNA interaction with endosomal TLRs-3,-7,-8 in siRNA transfer using conventional non-viral carriers [28,29]. Transfer of siRNA using Man-PEG_{2000} BLs and US exposure results in the direct deposition into the cytoplasm, and is not mediated by endocytosis (Fig. 1A and Supplementary Fig. 3C) [26]. Therefore, the inflammatory responses followed by the interaction with TLRs are expected to be low but siRNA is also recognized by cytoplasmic RIG-1/MDA-5 involved in inflammatory responses [30]. Since the modification of 3'-overhang sequences is suppressed by the activation of interferon-responsive factors (IRF)-3/7, transcriptional factors that exist downstream of RIG-1/MDA-5 pathway [31,32], we used siRNAs with 3'-dTdT overhang sequences (Supplementary Fig. 1A).

As shown in Figs. 1B-D and 3, ICAM-1 expression in LPS-stimulated HECs was significantly suppressed by ICAM-1 siRNA delivery using Man-PEG_{2000} BLs and US exposure, both *in vitro* and *in vivo*. Similarly, tissue infiltration of leukocytes and pro-inflammatory cytokine production were both suppressed following ICAM-1 suppression by siRNA delivery using this method (Fig. 4). Furthermore, potent anti-inflammatory effects were obtained by this ICAM-1 siRNA delivery in an LPS-stimulated inflammatory mouse model (Fig. 5). The delivery of siRNA to HECs, which express mannose receptors (Supplementary Fig. 4) [33], was selective and efficient using Man-PEG_{2000} BLs with US

exposure (Figs. 2B and 2C). Moreover, since a large amount of siRNA was directly transferred into the cytoplasm (Fig. 1A and Supplementary Fig. 3C) [26], endosomal escape and degradation within endosomes could be evaded. These data may indicate that nucleic acid transfer using Man-PEG_{2000} BLs and US exposure can be applied for siRNA delivery.

Although LPS is widely used to evaluate the induction of acute inflammatory responses, that are induced by not only various medicines but also surgical operation [34]. Aiming for the clinical application of anti-inflammatory therapy using our siRNA delivery method, the anti-inflammatory effects against various inflammatory models in mice were investigated. Following evaluation of the anti-inflammatory effects against CCl_4-, DMN-, and IR-stimulated inflammation, ICAM-1 expression in HECs and the inflammatory responses was significantly suppressed by ICAM-1 siRNA delivery using Man-PEG_{2000} BLs and US exposure in these inflammatory mouse models (Figs. 6-8 and Supplementary Figs. 6 and 7). Although the mechanisms of inflammatory responses as a result of LPS, CCl_4, DMN, and IR stimulation are different [5,6,35,36], ICAM-1 expression in HECs is reported in various types of inflammation, including drug-induced hepatic inflammation and IR-liver injury [7]. These data suggest that anti-inflammatory effects obtained by ICAM-1 siRNA delivery using Man-PEG_{2000} BLs and US exposure may be beneficial for acute hepatitis and liver injury.

In the present study, efficient ICAM-1 suppression was obtained at a dose of 1 μg siRNA/mouse (0.05 mg/kg) for siRNA delivery using Man-PEG_{2000} BLs and US exposure *in vivo* (Supplementary Fig. 5A). This dose of siRNA is lower than those reported for other studies evaluating the therapeutic effects using siRNA, although the therapeutic mechanism and delivery methods of each siRNA are likely to be different [37-39]. These findings suggest that the increased distribution of siRNA into HECs by mannose modification (Fig. 2) and the enhancement of intracytoplasmic siRNA transfer by sonoporation (Fig. 1A and

Supplementary Fig. 3) could contribute to the potent anti-inflammatory effects observed at a low dose of siRNA in our siRNA delivery method.

ICAM-1 suppression effects were only sustained for 72 h by siRNA delivery using Man-PEG_{2000} BLs and US exposure (Supplementary Fig. 5B). However, since the disease target of this study was acute inflammation, the potent therapeutic effects might be obtained in short duration and single administration of siRNA. Recently, it has been reported that ICAM-1 is involved in various diseases not only for acute/chronic hepatic failure, but also Crohn's disease, ulcerative colitis, and ileus [40-42]. In addition, antisense oligonucleotides against ICAM-1 (ISIS-2302; Alicaforsen) are currently under development for the treatment of Crohn's disease and ulcerative colitis [43,44]. However, most of these inflammatory diseases are based on "chronic" inflammation. In the present study, it is strongly suggested that transfer of ICAM-1 siRNA using Man-PEG_{2000} BLs and US exposure enables a large amount of siRNA to be delivered the cytoplasm of targeted cells (Fig. 1A and Supplementary Fig. 3). Therefore, to prolong the duration of gene suppression using this siRNA delivery system, future studies utilizing cholesterol-modified siRNA [45] or locked nucleic acid (LNA) [46], which are forms of stable siRNA resistant to enzymatic degradation, might be necessary for application to a variety of chronic inflammatory diseases.

Conclusions

In the present study, ICAM-1 siRNA was transferred into HECs selectively and efficiently, and sufficient ICAM-1 suppression effects were obtained by ICAM-1 siRNA transfer using Man-PEG_{2000} BLs and US exposure, both *in vitro* and *in vivo*. Moreover, potent anti-inflammatory effects were achieved against various types of inflammation by this ICAM-1 siRNA transfer. These findings contribute to overcoming the poor efficiency of

siRNA transfer into the cytoplasm of the targeted cells using non-viral carriers, and this novel siRNA delivery method using Man-PEG_{2000} BLs and US exposure may offer a valuable system for medical treatment where the cellular targets are HECs.

References

1. Verma S, Kaplowitz N. Diagnosis, management and prevention of drug-induced liver injury. Gut 2009;58:1555-1564.
2. Gurusamy KS, Gonzalez HD, Davidson BR. Current protective strategies in liver surgery. World J Gastroenterol 2010;16:6098-6103.
3. Freeman AJ, Dore GJ, Law MG, Thorpe M, Von Overbeck J, Lloyd AR, et al. Estimating progression to cirrhosis in chronic hepatitis C virus infection. Hepatology 2001;34:809-816.
4. Kuper H, Ye W, Broomé U, Romelsjö A, Mucci LA, Ekbom A, et al. The risk of liver and bile duct cancer in patients with chronic viral hepatitis, alcoholism, or cirrhosis. Hepatology 2001;34:714-718.
5. Tsuchiya H, Kaibori M, Yanagida H, Yokoigawa N, Kwon AH, Okumura T, et al. Pirfenidone prevents endotoxin-induced liver injury after partial hepatectomy in rats. J Hepatol 2004;40:94-101.
6. Teoh NC, Farrell GC. Hepatic ischemia reperfusion injury: pathogenic mechanisms and basis for hepatoprotection. J Gastroenterol Hepatol 2003;18:891-902.
7. Jaeschke H. Mechanisms of Liver Injury. II. Mechanisms of neutrophil-induced liver cell injury during hepatic ischemia-reperfusion and other acute inflammatory conditions. Am J Physiol Gastrointest Liver Physiol 2006;290:1083-1088.
8. Rijcken E, Krieglstein CF, Anthoni C, Laukoetter MG, Mennigen R, Spiegel HU, et al. ICAM-1 and VCAM-1 antisense oligonucleotides attenuate in vivo leucocyte adherence and inflammation in rat inflammatory bowel disease. Gut 2002;51:529-535.
9. Kono H, Uesugi T, Froh M, Rusyn I, Bradford BU, Thurman RG. ICAM-1 is involved in the mechanism of alcohol-induced liver injury: studies with knockout mice. Am J Physiol

Gastrointest Liver Physiol 2001;280:G1289-G1295.

10. Elbashir SM, Lendeckel W, Tuschl T. RNA interference is mediated by 21- and 22-nucleotide RNAs. Genes Dev 2001;15:188-200.
11. Elbashir SM, Harborth J, Lendeckel W, Yalcin A, Weber K, Tuschl T. Duplexes of 21-nucleotide RNAs mediate RNA interference in cultured mammalian cells. Nature 2001;411:494-498.
12. Sato A, Takagi M, Shimamoto A, Kawakami S, Hashida M. Small interfering RNA delivery to the liver by intravenous administration of galactosylated cationic liposomes in mice. Biomaterials 2007;28:1434-1442.
13. Kawakami S, Hashida M. Targeted delivery systems of small interfering RNA by systemic administration. Drug Metab Pharmacokinet 2007;22:142-151.
14. Mok H, Lee SH, Park JW, Park TG. Multimeric small interfering ribonucleic acid for highly efficient sequence-specific gene silencing. Nat Mater 2010;9:272-278.
15. Kim SS, Ye C, Kumar P, Chiu I, Subramanya S, Wu H, et al. Targeted delivery of siRNA to macrophages for anti-inflammatory treatment. Mol Ther 2010;18:993-1001.
16. Davis ME, Zuckerman JE, Choi CH, Seligson D, Tolcher A, Alabi CA, et al. Evidence of RNAi in humans from systemically administered siRNA via targeted nanoparticles. Nature 2010;464:1067-1070.
17. Takemoto H, Ishii A, Miyata K, Nakanishi M, Oba M, Ishii T, et al. Polyion complex stability and gene silencing efficiency with a siRNA-grafted polymer delivery system. Biomaterials 2010;31:8097-8105.
18. Higuchi Y, Kawakami S, Hashida M. Strategies for in vivo delivery of siRNAs: recent progress. BioDrugs 2010;24:195-205.
19. Hernot S, Klibanov AL. Microbubbles in ultrasound-triggered drug and gene delivery.

Adv Drug Deliv Rev 2008;60:1153-1166.

20. Li YS, Davidson E, Reid CN, McHale AP. Optimising ultrasound-mediated gene transfer (sonoporation) in vitro and prolonged expression of a transgene in vivo: potential applications for gene therapy of cancer. Cancer Lett 2009;273:62-69.
21. Lentacker I, Wang N, Vandenbroucke RE, Demeester J, De Smedt SC, Sanders NN. Ultrasound exposure of lipoplex loaded microbubbles facilitates direct cytoplasmic entry of the lipoplexes. Mol Pharm 2009;6:457-467.
22. Negishi Y, Matsuo K, Endo-Takahashi Y, Suzuki K, Matsuki Y, Takagi N, et al. Delivery of an angiogenic gene into ischemic muscle by novel bubble liposomes followed by ultrasound exposure. Pharm Res 2011;28:712-719.
23. Un K, Kawakami S, Suzuki R, Maruyama K, Yamashita F, Hashida M. Development of an ultrasound-responsive and mannose-modified gene carrier for DNA vaccine therapy. Biomaterials 2010;31:7813-7826.
24. Un K, Kawakami S, Suzuki R, Maruyama K, Yamashita F, Hashida M. Suppression of melanoma growth and metastasis by DNA vaccination using an ultrasound-responsive and mannose-modified gene carrier. Mol Pharm 2011;8:543-554.
25. Un K, Kawakami S, Higuchi Y, Suzuki R, Maruyama K, Yamashita F, et al. Involvement of activated transcriptional process in efficient gene transfection using unmodified and mannose-modified bubble lipoplexes with ultrasound exposure. J Control Release 2011; in press.
26. Un K, Kawakami S, Yoshida M, Higuchi Y, Suzuki R, Maruyama K, Yamashita F, Hashida M. The elucidation of gene transferring mechanism by ultrasound-responsive unmodified and mannose-modified lipoplexes. Biomaterials 2011;32:4659-4669.
27. Negishi Y, Endo Y, Fukuyama T, Suzuki R, Takizawa T, Omata D, et al. Delivery of

siRNA into the cytoplasm by liposomal bubbles and ultrasound. J Control Release 2008;132:124-130.

28. Matsushima H, Yamada N, Matsue H, Shimada S. TLR3-, TLR7-, and TLR9-mediated production of proinflammatory cytokines and chemokines from murine connective tissue type skin-derived mast cells but not from bone marrow-derived mast cells. J Immunol 2004;173:531-541.
29. Kawai T, Akira S. Toll-like receptor and RIG-I-like receptor signaling. Ann N Y Acad Sci 2008;1143:1-20.
30. Matsukura S, Kokubu F, Kurokawa M, Kawaguchi M, Ieki K, Kuga H, et al. Role of RIG-I, MDA-5, and PKR on the expression of inflammatory chemokines induced by synthetic dsRNA in airway epithelial cells. Int Arch Allergy Immunol 2007;143:80-83.
31. Marques JT, Devosse T, Wang D, Zamanian-Daryoush M, Serbinowski P, Hartmann R, et al. A structural basis for discriminating between self and nonself double-stranded RNAs in mammalian cells. Nat Biotechnol 2006;24:559-565.
32. Sato Y, Murase K, Kato J, Kobune M, Sato T, Kawano Y, et al. Resolution of liver cirrhosis using vitamin A-coupled liposomes to deliver siRNA against a collagen-specific chaperone. Nat Biotechnol 2008;26:431-442.
33. Elvevold K, Simon-Santamaria J, Hasvold H, McCourt P, Smedsrød B, Sørensen KK. Liver sinusoidal endothelial cells depend on mannose receptor-mediated recruitment of lysosomal enzymes for normal degradation capacity. Hepatology 2008;48:2007-2015.
34. Norris W, Paredes AH, Lewis JH. Drug-induced liver injury in 2007. Curr Opin Gastroenterol 2008;24:287-297.
35. Simeonova PP, Gallucci RM, Hulderman T, Wilson R, Kommineni C, Rao M, et al. The role of tumor necrosis factor-alpha in liver toxicity, inflammation, and fibrosis induced by

carbon tetrachloride. Toxicol Appl Pharmacol 2001;177:112-120.

36. Oyaizu T, Shikata N, Senzaki H, Matsuzawa A, Tsubura A. Studies on the mechanism of dimethylnitrosamine-induced acute liver injury in mice. Exp Toxicol Pathol 1997;49:375-380.
37. Song E, Lee SK, Wang J, Ince N, Ouyang N, Min J, et al. RNA interference targeting Fas protects mice from fulminant hepatitis. Nat Med 2003;9:347-351.
38. Yano J, Hirabayashi K, Nakagawa S, Yamaguchi T, Nogawa M, Kashimori I, et al. Antitumor activity of small interfering RNA/cationic liposome complex in mouse models of cancer. Clin Cancer Res 2004;10:7721-7726.
39. Zimmermann TS, Lee AC, Akinc A, Bramlage B, Bumcrot D, Fedoruk MN, et al. RNAi-mediated gene silencing in non-human primates. Nature 2006;441:111-114.
40. Yacyshyn BR, Schievella A, Sewell KL, Tami JA. Gene polymorphisms and serological markers of patients with active Crohn's disease in a clinical trial of antisense to ICAM-1. Clin Exp Immunol 2005;141:141-147.
41. Miner PB Jr, Geary RS, Matson J, Chuang E, Xia S, Baker BF, et al. Bioavailability and therapeutic activity of alicaforsen (ISIS 2302) administered as a rectal retention enema to subjects with active ulcerative colitis. Aliment Pharmacol Ther 2006;23:1427-1434.
42. The FO, Jonge WJ, Bennink RJ, van den Wijngaard RM, Boeckxstaens GE. The ICAM-1 antisense oligonucleotide ISIS-3082 prevents the development of postoperative ileus in mice. Br J Pharmacol 2005;146:252-258.
43. Yacyshyn BR, Chey WY, Goff J, Salzberg B, Baerg R, Buchman AL, et al. Double blind, placebo controlled trial of the remission inducing and steroid sparing properties of an ICAM-1 antisense oligodeoxynucleotide, alicaforsen (ISIS 2302), in active steroid dependent Crohn's disease. Gut 2002;51:30-36.

44. van Deventer SJ, Tami JA, Wedel MK. A randomised, controlled, double blind, escalating dose study of alicaforsen enema in active ulcerative colitis. Gut 2004;53:1646-1651.

45. Ambardekar VV, Han HY, Varney ML, Vinogradov SV, Singh RK, Vetro JA. The modification of siRNA with 3' cholesterol to increase nuclease protection and suppression of native mRNA by select siRNA polyplexes. Biomaterials 2011;32:1404-1411.

46. Elmén J, Thonberg H, Ljungberg K, Frieden M, Westergaard M, Xu Y, et al. Locked nucleic acid (LNA) mediated improvements in siRNA stability and functionality. Nucleic Acids Res 2005;33:439-447.

Figure Captions

Fig. 1. Suppression effects of *icam-1* mRNA expression and cytotoxicity followed by ICAM-1 siRNA delivery in LPS-stimulated primary mouse HECs. (A) *In vitro* confocal images of cellular associated ICAM-1 siRNA (1 μg siRNA) transferred by various methods at 1 h following treatment in primary mouse HECs. US was directly exposed to HECs at 5 min after addition of BLs. The lipoplexes were constructed with AlexaFluor-594 labeled ICAM-1 siRNA (red), and the endosomes were labeled with AlexaFluor-488 transferrin conjugates (green). Nuclei were counterstained with DAPI (blue). Scale bars, 10 μm. (B, C) The level of *icam-1* mRNA expression (B) and *in vitro* confocal images of ICAM-1 expression (C) obtained by ICAM-1 siRNA transfer (1 μg siRNA) using various types of methods at 24 h following LPS stimulation in primary mouse HECs. US was directly exposed to HECs at 5 min after addition of BLs, and cells were exposed to LPS (100 ng/mL) at 24 h after the addition of siRNA or lipoplexes/BLs. ICAM-1 was labeled with anti-mouse ICAM-1 antibody and FITC-conjugated secondary antibody (green), and nuclei were counterstained by DAPI (blue). Scale bars, 10 μm. (D, E) Comparison of the suppression of *icam-1* mRNA expression (D) and cell viability (E) obtained by siRNA transfer using Man-PEG_{2000} BLs (1 μg siRNA) and US exposure with that by Lipofectamine 2000. $^{*}P<0.05$; $^{**}P<0.01$, compared with N.T.. Each value represents the mean+SD (n=5). N.T., no treatment.

Fig. 2. *In vivo* distribution of ICAM-1 siRNA delivered by Man-PEG_{2000} BLs and US exposure. (A) Tissue distribution and pharmacokinetics of radio-labeled bare- and Man-PEG_{2000} BLs complexed with 10 μg ICAM-1 siRNA after i.v. administration into mice. Tissue distribution of lipoplexes was measured at 6 h after i.v. administration of lipoplexes. Inset shows blood concentration of lipoplexes at predetermined times after i.v. administration.

$^{*}P<0.05$, $^{**}P<0.01$, compared with the corresponding group of bare-PEG_{2000} lipoplexes. Each value represents the mean±SD (n=5). (B) Hepatic cellular localization of AlexaFluor-594 labeled ICAM-1 siRNA delivered by bare- and Man-PEG_{2000} BLs (10 μg siRNA) and US exposure at 6 h after i.v. administration of lipoplexes into mice. Liver was separated to hepatocytes, Kupffer cells, and endothelial cells by collagenase perfusion, one-step density gradient centrifugation, and magnetic cell sorting according to *Supplementary Materials and Methods*. $^{**}P<0.01$, compared with the corresponding group of hepatocytes. Each value represents the mean+SD (n=5). (C) Fluorescent images of hepatic localization of AlexaFluor-594 labeled ICAM-1 siRNA (red) delivered by bare- and Man-PEG_{2000} BLs (10 μg siRNA) and US exposure. HECs were labeled with anti-mouse CD146 antibody and FITC-conjugated secondary antibody (green), and nuclei were counterstained with DAPI (blue). Livers were harvested at 6 h after i.v. administration of lipoplexes into mice, and magnified images corresponding to the areas enclosed in boxes are presented in (i). Scale bars, 100 μm.

Fig. 3. Suppression effects of ICAM-1 siRNA delivery using Man-PEG_{2000} BLs and US exposure on *icam-1* mRNA and protein expression in HECs of an LPS/D-galactosamine-induced inflammatory mouse model. (A) Evaluation schedule of ICAM-1 expression in LPS/D-galactosamine-stimulated mice. (B, C, D) The expression level of *icam-1* mRNA in cells (B) and protein on the cell membrane (C, D) obtained by siRNA delivery (10 μg siRNA) using various methods in HECs. At 24 h after siRNA delivery, LPS/D-galactosamine (1 μg/100 mg/kg) was i.p. administered into mice to induce the acute inflammatory responses. HECs were isolated by collagenase perfusion, one-step density gradient centrifugation, and magnetic cell sorting according to *Supplementary Materials and*

Methods. The *icam-1* mRNA and protein expression in HECs was determined by quantitative RT-PCR (B), western blotting/ELISA (C), and confocal images (D). The expression levels of mRNA and protein were detected at 3 and 6 h following LPS/D-galactosamine stimulation, respectively. $^{*}P<0.05$; $^{**}P<0.01$, compared with N.T.. Each value represents the mean+SD (n=5). ICAM-1 was labeled with anti-mouse ICAM-1 antibody and FITC-conjugated secondary antibody (green), and nuclei were counterstained with DAPI (blue). Scale bars, 100 μm. N.T., no treatment.

Fig. 4. Suppression effects of ICAM-1 siRNA delivery using Man-PEG_{2000} BLs and US exposure on leukocyte infiltration and pro-inflammatory cytokine production in an LPS/D-galactosamine-induced inflammatory mouse model. (A) Evaluation schedule of leukocyte infiltration and pro-inflammatory cytokine production in LPS/D-galactosamine-stimulated mice. (B, C) The levels of IL-8 and MCP-1 expression in the liver (B) and the levels of TNF-α, IFN-γ, and IL-6 secretion in the serum (C) following siRNA delivery (10 μg siRNA) using various delivery methods at 12 h following LPS/D-galactosamine stimulation. $^{**}P<0.01$, compared with N.T.. Each value represents the mean+SD (n=5). N.T., no treatment. (D) Photomicrographs of infiltrated leukocytes following siRNA delivery using Man-PEG_{2000} BLs (10 μg siRNA) and US exposure in LPS/D-galactosamine-stimulated mouse liver. Leukocytes were labeled with anti-mouse Gr-1 (Ly-6G) antibody and RITC-conjugated secondary antibody (red), and nuclei were counterstained with DAPI (blue). Scale bars, 100 μm. $^{**}P<0.01$, compared with N.T.. Each value represents the mean+SD (n=5). N.T., no treatment.

Fig. 5. Suppression effects of ICAM-1 siRNA delivery using Man-PEG_{2000} BLs and US

exposure on liver toxicity in an LPS/D-galactosamine-induced inflammatory mouse model. (A) The level of serum ALT/AST activities following by siRNA delivery (10 μg siRNA) using various methods at predetermined times after LPS/D-galactosamine stimulation. Each value represents the mean±SD (n=5). (B) Fluorescent images of apoptosis following by siRNA delivery using Man-PEG_{2000} BLs (10 μg siRNA) and US exposure in LPS/D-galactosamine-stimulated mice. Apoptosis (green) was detected by TUNEL staining, and nuclei were counterstained with DAPI (blue). Scale bars, 100 μm. (C) Liver histology with H&E staining at 24 h following siRNA delivery using Man-PEG_{2000} BLs (10 μg siRNA) and US exposure in LPS/D-galactosamine-induced inflammatory mouse model. Black arrows: destruction of tube formation in hepatic central vein. Scale bars, 100 μm.

Fig. 6. Suppression effects of ICAM-1 siRNA delivery using Man-PEG_{2000} BLs and US exposure on *icam-1* mRNA and protein expression in HECs of an IR-induced hepatic inflammatory mouse model. (A) Evaluation schedule of ICAM-1 expression in hepatic IR-stimulated mice. (B, C) The expressing level of *icam-1* mRNA in the cells (B) and protein on the cell membrane (C) obtained by siRNA delivery (10 μg siRNA) using various delivery methods in HECs. HECs were isolated by collagenase perfusion, one-step density gradient centrifugation, and magnetic cell sorting according to *Supplementary Materials and Methods*. The *icam-1* mRNA and protein expression in HECs was determined by quantitative RT-PCR (B), western blotting/ELISA (C). The expression levels of mRNA and protein were detected at 3 and 6 h following IR-stimulation, respectively. $^{*}P<0.05$; $^{**}P<0.01$, compared with sham operation. Each value represents the mean+SD (n=5).

Fig. 7. Suppression effects of ICAM-1 siRNA delivery using Man-PEG_{2000} BLs and US

exposure on leukocyte infiltration and pro-inflammatory cytokine production in IR-induced hepatic inflammatory mouse model. (A) Evaluation schedule of leukocyte infiltration and pro-inflammatory cytokine production in hepatic IR-stimulated mice. (B, C) The levels of IL-8, MCP-1 expression in the liver (B) and TNF-α, IFN-γ, IL-6 secretion in the serum (C) following by siRNA delivery (10 μg siRNA) using various delivery methods at 6 h following IR-stimulation. $^{**}P<0.01$, compared with sham operation. Each value represents the mean+SD (n=5).

Fig. 8. Suppression effects of ICAM-1 siRNA delivery using Man-PEG_{2000} BLs and US exposure on liver toxicity in an IR-induced hepatic inflammatory mouse model. (A) The level of serum ALT/AST activities followed by siRNA delivery (10 μg siRNA) using various delivery methods at 24 h following hepatic IR-stimulation. $^{**}P<0.01$, compared with the corresponding sham operation group. Each value represents the mean+SD (n=5). (B) Fluorescent images of apoptosis followed by siRNA delivery using Man-PEG_{2000} BLs (10 μg siRNA) and US exposure in IR-induced hepatic inflammatory mouse model. Apoptosis (green) was detected by TUNEL staining, and nuclei were counterstained with DAPI (blue). Scale bars, 100 μm. (C) Liver histology at 24 h following siRNA delivery using Man-PEG_{2000} BLs (10 μg siRNA) and US exposure in IR-induced hepatic inflammatory mouse model. Black arrows: destruction of tube formation in hepatic central vein. Scale bars, 100 μm.

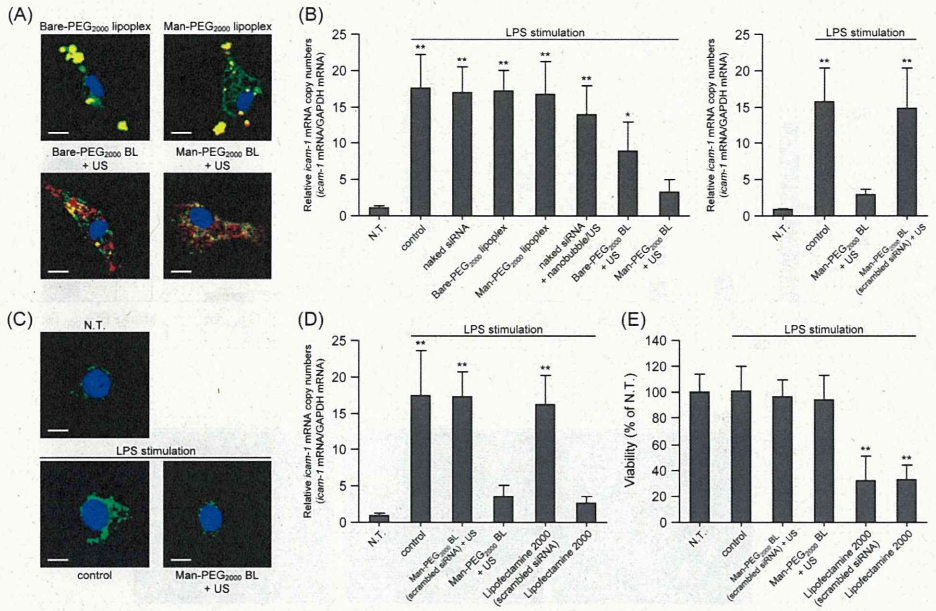

Fig. 1. Suppression effects of *icam-1* mRNA expression and cytotoxicity followed by ICAM-1 siRNA delivery in LPS-stimulated primary mouse HECs. (A) *In vitro* confocal images of cellular associated ICAM-1 siRNA (1 μg siRNA) transferred by various methods at 1 h following treatment in primary mouse HECs. US was directly exposed to HECs at 5 min after addition of BLs. The lipoplexes were constructed with AlexaFluor-594 labeled ICAM-1 siRNA (red), and the endosomes were labeled with AlexaFluor-488 transferrin conjugates (green). Nuclei were counterstained with DAPI (blue). Scale bars, 10 μm. (B, C) The level of *icam-1* mRNA expression (B) and *in vitro* confocal images of ICAM-1 expression (C) obtained by ICAM-1 siRNA transfer (1 μg siRNA) using various types of methods at 24 h following LPS stimulation in primary mouse HECs. US was directly exposed to HECs at 5 min after addition of BLs, and cells were exposed to LPS (100 ng/mL) at 24 h after the addition of siRNA or lipoplexes/BLs. ICAM-1 was labeled with anti-mouse ICAM-1 antibody and FITC-conjugated secondary antibody (green), and nuclei were counterstained by DAPI (blue). Scale bars, 10 μm. (D, E) Comparison of the suppression of *icam-1* mRNA expression (D) and cell viability (E) obtained by siRNA transfer using Man-PEG_{2000} BLs (1 μg siRNA) and US exposure with that by Lipofectamine 2000. $^{*}P<0.05$; $^{**}P<0.01$, compared with N.T.. Each value represents the mean+SD (n=5). N.T., no treatment.

93x61mm (600 x 600 DPI)

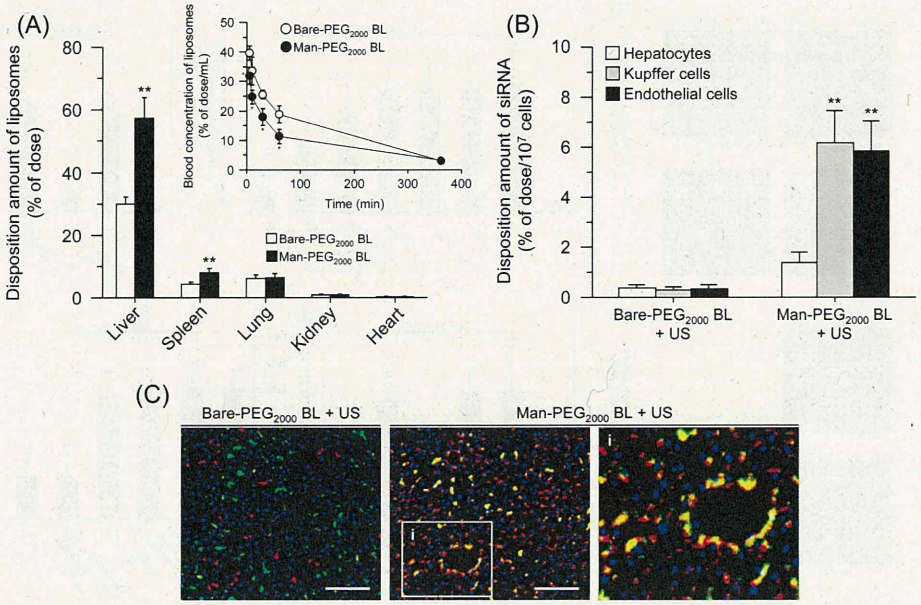

Fig. 2. *In vivo* distribution of ICAM-1 siRNA delivered by Man-PEG_{2000} BLs and US exposure. (A) Tissue distribution and pharmacokinetics of radio-labeled bare- and Man-PEG_{2000} BLs complexed with 10 μg ICAM-1 siRNA after i.v. administration into mice. Tissue distribution of lipoplexes was measured at 6 h after i.v. administration of lipoplexes. Inset shows blood concentration of lipoplexes at predetermined times after i.v. administration. $^{*}P<0.05$, $^{**}P<0.01$, compared with the corresponding group of bare-PEG_{2000} lipoplexes. Each value represents the mean±SD (n=5). (B) Hepatic cellular localization of AlexaFluor-594 labeled ICAM-1 siRNA delivered by bare- and Man-PEG_{2000} BLs (10 μg siRNA) and US exposure at 6 h after i.v. administration of lipoplexes into mice. Liver was separated to hepatocytes, Kupffer cells, and endothelial cells by collagenase perfusion, one-step density gradient centrifugation, and magnetic cell sorting according to *Supplementary Materials and Methods*. $^{**}P<0.01$, compared with the corresponding group of hepatocytes. Each value represents the mean+SD (n=5). (C) Fluorescent images of hepatic localization of AlexaFluor-594 labeled ICAM-1 siRNA (red) delivered by bare- and Man-PEG_{2000} BLs (10 μg siRNA) and US exposure. HECs were labeled with anti-mouse CD146 antibody and FITC-conjugated secondary antibody (green), and nuclei were counterstained with DAPI (blue). Livers were harvested at 6 h after i.v. administration of lipoplexes into mice, and magnified images corresponding to the areas enclosed in boxes are presented in (i). Scale bars, 100 μm.
92x61mm (600 x 600 DPI)

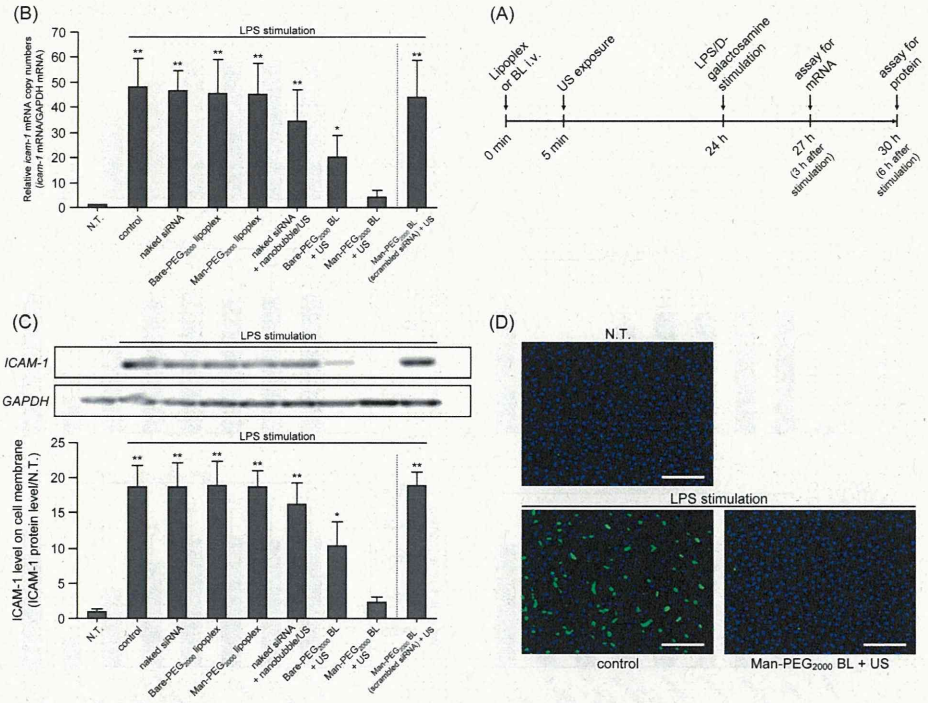

Fig. 3. Suppression effects of ICAM-1 siRNA delivery using Man-PEG_{2000} BLs and US exposure on *icam-1* mRNA and protein expression in HECs of an LPS/D-galactosamine-induced inflammatory mouse model. (A) Evaluation schedule of ICAM-1 expression in LPS/D-galactosamine-stimulated mice. (B, C, D) The expression level of *icam-1* mRNA in cells (B) and protein on the cell membrane (C, D) obtained by siRNA delivery (10 μg siRNA) using various methods in HECs. At 24 h after siRNA delivery, LPS/D-galactosamine (1 μg/100 mg/kg) was i.p. administered into mice to induce the acute inflammatory responses. HECs were isolated by collagenase perfusion, one-step density gradient centrifugation, and magnetic cell sorting according to *Supplementary Materials and Methods*. The *icam-1* mRNA and protein expression in HECs was determined by quantitative RT-PCR (B), western blotting/ELISA (C), and confocal images (D). The expression levels of mRNA and protein were detected at 3 and 6 h following LPS/D-galactosamine stimulation, respectively. $^{*}P<0.05$; $^{**}P<0.01$, compared with N.T.. Each value represents the mean+SD (n=5). ICAM-1 was labeled with anti-mouse ICAM-1 antibody and FITC-conjugated secondary antibody (green), and nuclei were counterstained with DAPI (blue). Scale bars, 100 μm. N.T., no treatment.
106x81mm (600 x 600 DPI)

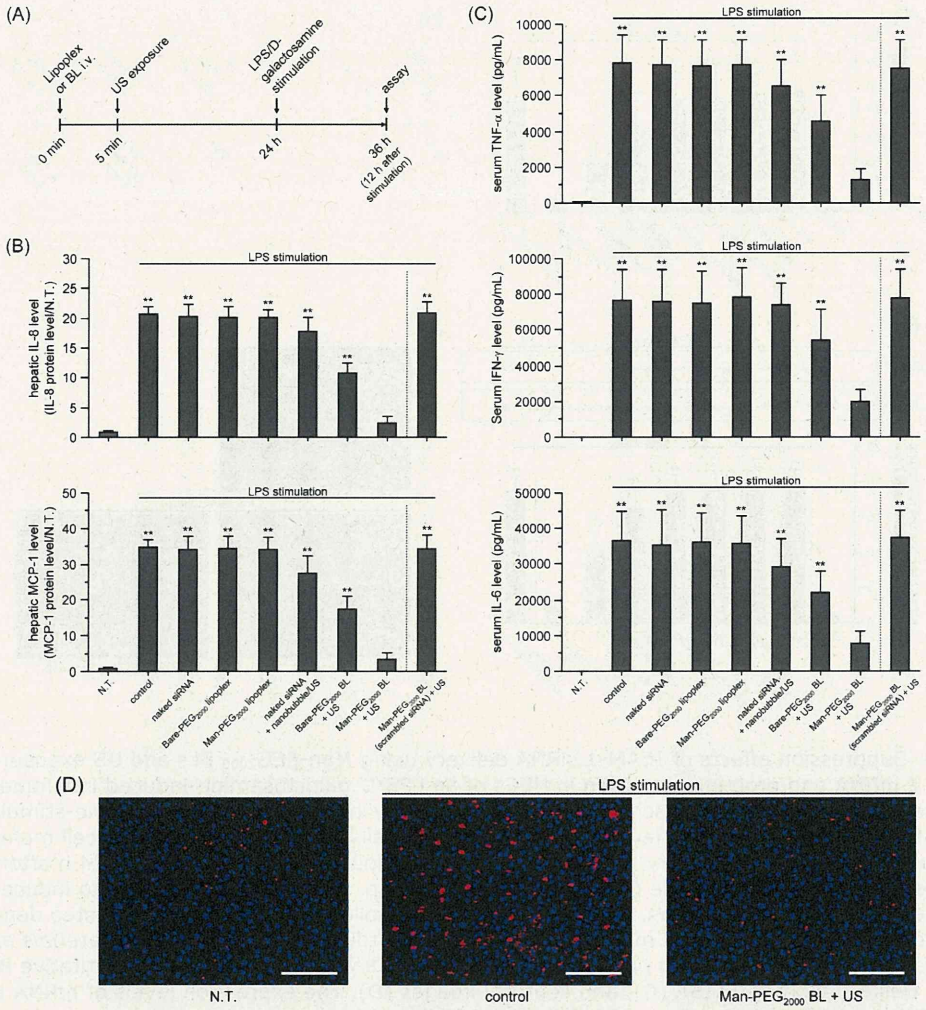

Fig. 4. Suppression effects of ICAM-1 siRNA delivery using Man-PEG_{2000} BLs and US exposure on leukocyte infiltration and pro-inflammatory cytokine production in an LPS/D-galactosamine-induced inflammatory mouse model. (A) Evaluation schedule of leukocyte infiltration and pro-inflammatory cytokine production in LPS/D-galactosamine-stimulated mice. (B, C) The levels of IL-8 and MCP-1 expression in the liver (B) and the levels of TNF-α, IFN-γ, and IL-6 secretion in the serum (C) following siRNA delivery (10 μg siRNA) using various delivery methods at 12 h following LPS/D-galactosamine stimulation. $^{**}P<0.01$, compared with N.T.. Each value represents the mean+SD (n=5). N.T., no treatment. (D) Photomicrographs of infiltrated leukocytes following siRNA delivery using Man-PEG_{2000} BLs (10 μg siRNA) and US exposure in LPS/D-galactosamine-stimulated mouse liver. Leukocytes were labeled with anti-mouse Gr-1 (Ly-6G) antibody and RITC-conjugated secondary antibody (red), and nuclei were counterstained with DAPI (blue). Scale bars, 100 μm. $^{**}P<0.01$, compared with N.T.. Each value represents the mean+SD (n=5). N.T., no treatment.
130x141mm (600 x 600 DPI)